

# Model Predictive Pulse Pattern Control

Tobias Geyer, *Senior Member, IEEE*, Nikolaos Oikonomou, *Member, IEEE*,  
Georgios Papafotiou, *Member, IEEE*, and Frederick Kieferndorf, *Member, IEEE*

**Abstract**—Industrial applications of medium-voltage drives impose increasingly stringent performance requirements, particularly with regards to harmonic distortions of the phase currents of the controlled electrical machine. An established method to achieve very low current distortions during steady-state operation is to employ offline calculated optimized pulse patterns (OPP). Achieving high dynamic performance, however, proves to be very difficult in a system operated by OPPs.

In this paper, we propose a method that combines the optimal steady-state performance of OPPs with the very fast dynamics of trajectory tracking control. A constrained optimal control problem with a receding horizon policy, i.e. model predictive control (MPC), is formulated and solved. Results show that the combination of MPC with OPPs satisfies both the strict steady-state as well as the dynamic performance requirements imposed by the most demanding industrial applications. The estimation of the fundamental components of the machine variables separately from their respective harmonic components is not required. As a result, complicated structures such as observers can be avoided, contrary to state-of-the-art methods. A further advantage of the MPC method is the use of a receding horizon policy, which provides feedback and a high degree of robustness.

**Index Terms**—AC motor drives, optimized pulse patterns, pulse width modulation, trajectory tracking control, model predictive control

## I. INTRODUCTION

Medium-voltage ac drives are operated at low switching frequencies to minimize the switching losses of the power semiconductors in the inverter. However, lowering the switching frequency typically increases the harmonic distortions of the machine's currents, resulting in high harmonic losses. One solution is to employ offline calculated pulse patterns to control the commanding power inverter; such patterns minimize the current harmonics for a given switching frequency.

Traditionally, however, it has only been possible to use optimized pulse patterns (OPPs) in a modulator driven by a very slow control loop. This leads to a poor dynamic performance and to harmonic excursions of the stator currents when the operating point is changed or when transitions between different pulse patterns occur.

This paper describes a novel control and modulation strategy, based on OPPs, that enables very fast response times during transients, a fast rejection of disturbances, and a nearly optimal ratio of harmonic current distortion per switching frequency at steady-state operation. These OPPs are computed

in an offline procedure by calculating the switching angles over a quarter fundamental period for all possible operating points [1]–[3]. Typically, the objective is to minimize the total harmonic distortion (THD) of the current for a given switching frequency.

A common method to establish control in closed loop is to use field oriented control (FOC). In this case, the performance of the overall control scheme is very limited—even in quasi steady-operation—when OPPs are employed for pulse width modulation. Excursions of the harmonic currents occur that may lead to overcurrent conditions [4]. Thus, the application of field oriented current control with OPPs is typically limited to grid-connected setups, where the operating range is relatively small. When the goal is to use this method in applications with widely varying operating points, as is the case for electrical machine control, the (inner) current control loop is tuned to be very slow, such that its operation does not interfere with the optimal volt-second balance of the OPPs. However, such a tuning significantly decreases the dynamic performance of the drive.

Furthermore, in the above mentioned case, the offline optimization procedure of OPPs itself is compromised, by adding restrictions to the optimization algorithm that reduce the number of discontinuities between neighboring pulse patterns, i.e. between switching angles that correspond to different values of the modulation index and/or different values of the pulse number. Eliminating these discontinuities in the OPP allows for satisfactory operation at quasi steady-state by eliminating a priori the possibility of harmonic excursions when the operating point changes. However, the resulting currents are suboptimal in terms of the THD even at steady-state operation, because of the additional restrictions added during the offline optimization procedure.

As an improvement to FOC with OPPs, *current trajectory tracking* was proposed in [5], [6]. This method derives the optimal steady-state stator current trajectory from the pulse pattern in use. The actual stator current space vector is forced to follow this target trajectory. A disadvantage is that the stator current trajectory depends on the parameters of the electrical machine, specifically on the total leakage inductance [7]. Changing load conditions have also been found to influence the stator current trajectory.

A further improvement can be made by tracking the *stator flux trajectory* [8], which is insensitive to parameter variations and is thus better suited for tracking control. By controlling the stator flux space vector to coincide with its optimal trajectory, harmonic excursions are avoided that might appear when the operating point changes. The method requires an observer to

T. Geyer is currently with the Department of Electrical and Computer Engineering, The University of Auckland, New Zealand; e-mail: t.geyer@ieee.org. N. Oikonomou, G. Papafotiou and F. Kieferndorf are with ABB Corporate Research, Baden-Dättwil, Switzerland; e-mails: nikolaos.oikonomou@ch.abb.com, georgios.papafotiou@ch.abb.com and frederick.kieferndorf@ch.abb.com

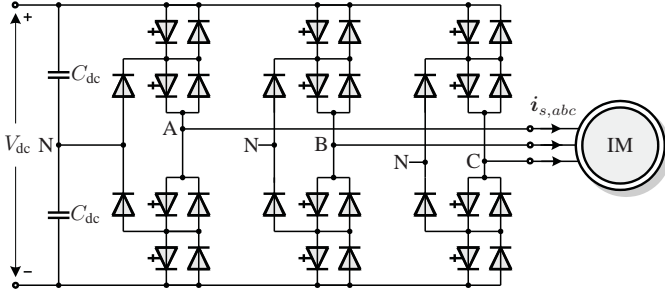


Fig. 1: Three-level neutral point clamped VSI driving an induction machine

establish control in closed loop. This observer identifies the instantaneous fundamental components of the stator current and flux linkage vectors in real-time [9]. These signals are not readily available when using OPPs [7], since the harmonic current is not zero at the sampling instants. As a result, the fundamental machine quantities cannot be directly sampled when using OPPs. This makes the design of the closed-loop controller difficult, because these signals are required to achieve flux and torque control. For this reason, existing control schemes, such as [5], [10], employ an observer to derive the instantaneous fundamental current and flux linkage values separately from the respective harmonic quantities.

For reliability, simplicity of implementation and dynamic performance reasons, the following three aims are targeted: First, it is desired to perform trajectory tracking control of the stator flux vector without the need of estimating the fundamental component of the stator flux or current in real-time. Second, the controller should have reduced sensitivity to parameter variations and measurement noise. Third, fast dynamic control is to be achieved while performing the minimum possible modification of the offline calculated pulse pattern sequences. These three objectives are achieved by the controller proposed in this paper. The stator flux trajectory controller is generalized, by formulating it as a constrained optimal control problem with a receding horizon policy, i.e. as model predictive control (MPC) [11]–[13]. We refer to this concept as *model predictive pulse pattern control* (MP<sup>3</sup>C).

Specifically, a prediction horizon of finite length in time is used and the switching instants of the pulse pattern are shifted such that a stator flux error is corrected within this horizon. From the end of the horizon onwards, steady-state operation is assumed. The underlying optimization problem is solved in real-time, yielding a sequence of optimal control actions over the horizon. Only the *first* control action of this sequence is applied to the drive system, in accordance with the so-called receding horizon policy. At the next sampling instant, the control sequence is recomputed over a shifted horizon, thus providing feedback and robustness to model inaccuracies. A long horizon also renders the controller less susceptible to measurement noise. The receding horizon policy is illustrated in Fig. 2.

The paper is organized as follows. Section II highlights the drive system case study considered in this paper, and Section III summarizes the offline computation and characteristics

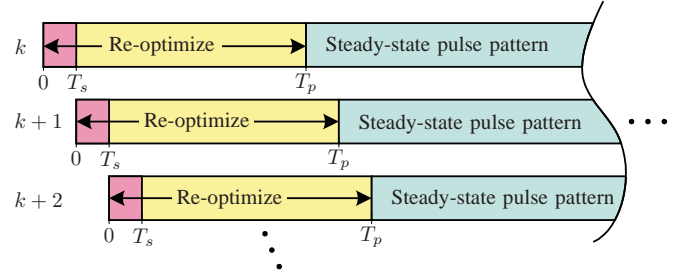


Fig. 2: Illustration of the receding horizon policy. The pulse pattern is re-optimized over the prediction horizon  $T_p$ , but only the pattern over the sampling interval  $T_s$  is applied to the drive

of OPPs. Section IV describes the proposed pulse pattern controller in detail. The underlying optimization problem constitutes a quadratic program (QP), which can be solved efficiently in real time by approximation, as shown in Section V. It is also shown that a further simplification yields a deadbeat (DB) trajectory controller. Section VI evaluates the performance under steady-state operating conditions and during transients, and compares it with carrier-based pulse width modulation (CB-PWM) and space vector modulation (SVM). The impact of flux observer noise and machine parameter variations are investigated. Conclusions are provided in Section VII.

## II. DRIVE SYSTEM CASE STUDY

Throughout this paper, we will use normalized quantities. All variables  $\xi_{abc} = [\xi_a \ \xi_b \ \xi_c]^T$  in the three-phase system ( $abc$ ) are transformed to  $\xi_{\alpha\beta} = [\xi_\alpha \ \xi_\beta]^T$  in the stationary orthogonal  $\alpha\beta$  coordinates through  $\xi_{\alpha\beta} = \mathbf{P} \xi_{abc}$  with

$$\mathbf{P} = \frac{2}{3} \begin{bmatrix} 1 & -\frac{1}{2} & -\frac{1}{2} \\ 0 & \frac{\sqrt{3}}{2} & -\frac{\sqrt{3}}{2} \end{bmatrix}, \quad \mathbf{P}^{-1} = \begin{bmatrix} 1 & 0 \\ -\frac{1}{2} & \frac{\sqrt{3}}{2} \\ -\frac{1}{2} & -\frac{\sqrt{3}}{2} \end{bmatrix}. \quad (1)$$

$\mathbf{P}^{-1}$  denotes the pseudo-inverse of  $\mathbf{P}$ .

As an illustrative example of a medium-voltage variable speed drive system consider a three-level neutral point clamped (NPC) voltage source inverter (VSI) driving an induction machine (IM), as depicted in Fig. 1. The total dc-link voltage  $V_{dc}$  over the two dc-link capacitors  $C_{dc}$  is assumed to be constant.

Let the integer variables  $u_a, u_b, u_c \in \{-1, 0, 1\}$  denote the switch positions in each phase leg, where the values  $-1, 0, 1$  correspond to the phase voltages  $-\frac{V_{dc}}{2}, 0, \frac{V_{dc}}{2}$ , respectively. The actual voltage applied to the machine terminals is given by  $\mathbf{u}_{\alpha\beta} = 0.5V_{dc} \mathbf{P} \mathbf{u}_{abc}$  with  $\mathbf{u}_{abc} = [u_a \ u_b \ u_c]^T$ .

## III. OPTIMIZED PULSE PATTERNS

### A. Offline Computation

When computing OPPs, a single-phase pulse pattern is typically considered and quarter-wave symmetry is imposed. To compute the single-phase OPP over 90 degrees, the number of primary switching angles (the pulse number)  $d$  needs to be selected. Fig. 3(a) shows an example for a three-level switching sequence with  $d = 5$ . An objective function is chosen for

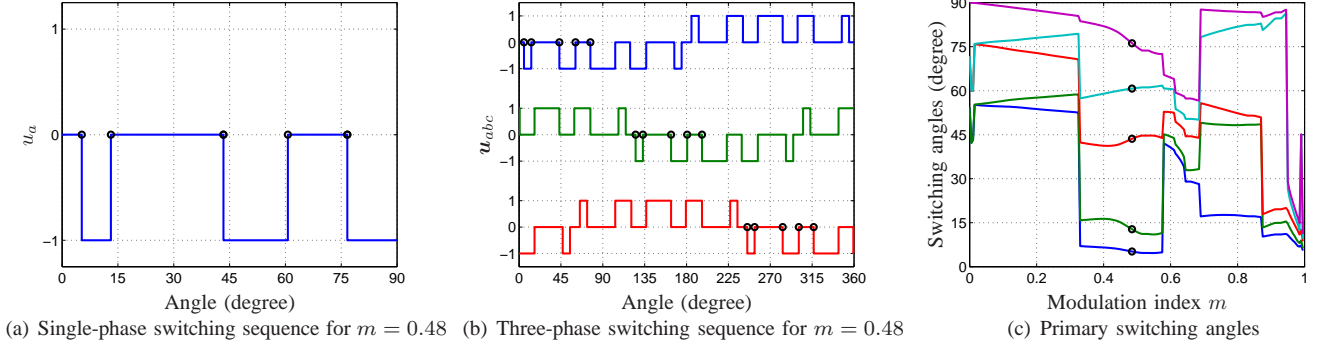


Fig. 3: Optimal pulse pattern with  $d = 5$  primary switching angles for a three-level inverter. The single-phase and three-phase switching sequences correspond to the modulation index  $m = 0.48$ . The primary switching angles are indicated by (black) circles

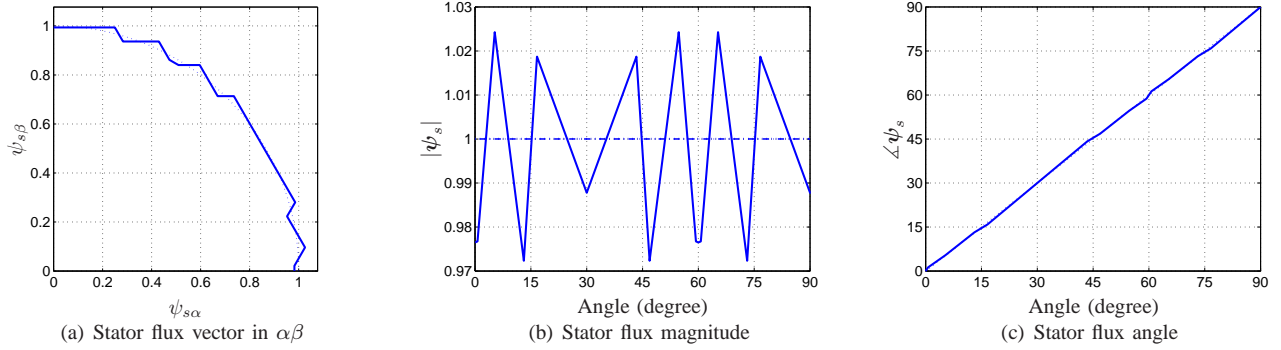


Fig. 4: Stator flux trajectory, magnitude and angle for the optimal pulse pattern shown in Fig. 3. The dashed lines refer to the reference values

the optimization—a common selection is the weighted sum of the squared differential-mode voltage harmonics, which is effectively equivalent to the total harmonic distortion (THD) of the current. For every value of the modulation index, this objective function is minimized by optimizing over the switching angles. This leads to a set of switching angles as a function of the modulation index, characterizing the OPP as shown in Fig. 3(c).

Starting from the single-phase switching sequence over 90 degrees shown in Fig. 3(a), the three-phase pulse pattern is obtained by applying the quarter-wave symmetry and by shifting the single-phase pattern by 0, 120 and 240 degrees, respectively. This leads to the pulse pattern shown in Fig. 3(b). As a result, the three-phase pulse pattern over 360 degrees is fully characterized by the single-phase pattern over 90 degrees. For more details on the computation of OPPs for multi-level inverters, see for example [14].

### B. Stator Flux Trajectory

Consider an electrical machine connected to the inverter terminals and neglect the machine's stator resistance. The steady-state stator flux trajectory in stationary coordinates, which corresponds to the OPP in use, is obtained by integrating the switched voltage sequence  $\mathbf{u}_{\alpha\beta}$  over time. Specifically, the

stator flux vector  $\boldsymbol{\psi}_s = [\psi_{s\alpha} \ \psi_{s\beta}]^T$  at time  $t$  is given by

$$\boldsymbol{\psi}_s(t) = \boldsymbol{\psi}_s(0) + \frac{V_{dc}}{2} \int_0^t \mathbf{P} \mathbf{u}_{abc}(\tau) d\tau. \quad (2)$$

An example steady-state stator flux trajectory in stationary coordinates is shown in Fig. 4(a) over 90 degrees. The average amplitude of the stator flux trajectory is one, yet it is obvious from Fig. 4(a) that the instantaneous amplitude of the stator flux oscillates, as shown in Fig. 4(b). The instantaneous angle of the stator flux vector also oscillates around its nominal value, see Fig. 4(c). This ripple is the result of variations in the instantaneous angular speed of the stator flux vector, which necessarily arise when applying voltage vectors of different and discrete magnitudes. The ripples on the magnitude and angle of the stator flux vector, which repeats itself every 60 degrees and also exhibits a 30 degree symmetry, dictate the discrete frequency spectrum of the current harmonics.

### C. Properties

The result of this offline computation is a look-up table that holds the switching (firing) angles for the semiconductor switches and the respective phase potential values. The content of this look-up table is a function of the modulation index, a normalized quantity that is proportional to the magnitude of the reference voltage in the linear operating range.

A basic property of OPPs should be explained. Pulse width modulation by OPPs is characterized by an integer number

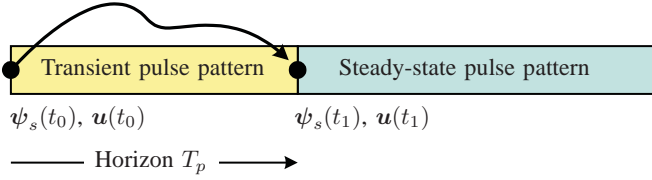


Fig. 5: Boundary control problem formulated over the horizon  $T_p$ . The transient pulse pattern drives the stator flux vector  $\psi_s$  from time  $t_0$  to  $t_1$  and links the switch positions  $u$

of switching events over one fundamental period of the stator voltage waveform, which is the pulse number  $d$ . As a result, the switched waveform is synchronized to the fundamental voltage waveform at all operating points and load conditions. Therefore, modulation by OPPs belongs to the class of synchronous PWM methods. This synchronization property of OPPs comes with one advantage and one disadvantage.

Owing to the synchronism between the pulse pattern and the fundamental waveform, subharmonic spectral components do not exist. Moreover, all integer harmonics of even order and all triplen harmonics are zero. The latter is true, because quarter-wave symmetry is typically assumed when calculating OPPs for a three-phase system. The result is a discrete-frequency spectrum, which only comprises the integer components of order 1, 5, 7, 11, 13, etc.

However, the synchronization of OPPs to the fundamental period of the voltage implies the lack of a symmetrical modulation cycle [15]. The latter is commonly defined as a time interval of fixed length during which the reference voltage is approximated by the applied sequence of switching state vectors. A symmetrical modulation cycle of fixed length is a typical feature of carrier-based PWM and space vector modulation (SVM). Its symmetry ensures that the trajectory of the resulting harmonic current describes a closed pattern centered in the origin of the complex plane. This feature allows the sampling of the current at regular time intervals, equal to the half of the modulation cycle: by performing such sampling, only the fundamental component of the current is obtained; the harmonic current is zero at the sampling instants. This property does not exist when using OPPs to synthesize the voltage [10], making it difficult to establish torque and flux control in systems operated with OPPs: sampling the current at time instants when the harmonic content is non-zero results in distortions perpetuating the closed loop and affecting adversely the control action. This adverse effect is particularly pronounced in medium-voltage drives operated at low switching frequencies.

#### IV. MODEL PREDICTIVE PULSE PATTERN CONTROL

Closed-loop control of an electrical machine based on OPPs can be achieved by controlling the stator flux vector along its reference trajectory. The magnitude of the stator flux trajectory determines the magnetization current of the machine, while the angle between the stator and the rotor flux vectors determines the electromagnetic torque.

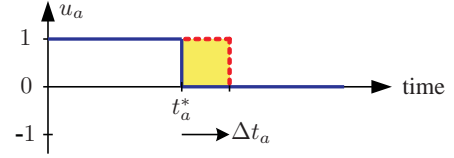


Fig. 6: Delaying the negative switching transition  $\Delta u_a = -1$  in phase  $a$  by  $\Delta t_a$ , with regards to the nominal switching time  $t_a^*$ , increases the stator flux component in this phase by  $0.5V_{dc}(-\Delta u_a)\Delta t_a$

The flux error vector is the vector difference between the reference flux trajectory and the actual trajectory of the stator flux of the machine. Even at steady-state, this flux error vector is generally non-zero due to non-idealities of the real-world drive system. These non-idealities include fluctuations in the dc-link voltage, the presence of the stator resistance, neglected in (2), and non-idealities of the power inverter, such as dead-time effects. During transient operation, the flux error vector is an accurate mapping of the change in the operating point.

##### A. Stator Flux Control Problem

The stator flux control problem can be interpreted as a boundary control problem, as illustrated in Fig. 5. Starting at time  $t_0$  with the switch position  $u(t_0)$  and the stator flux  $\psi_s(t_0)$ , a *transient* pulse pattern over the time-interval  $T_p$  is to be derived. This pulse pattern drives the stator flux vector to the terminal stator flux  $\psi_s(t_1)$  and leads to the terminal switch position  $u(t_1)$ . In this boundary control problem,  $u(t_0)$  and  $\psi_s(t_0)$  are the initial conditions, while  $u(t_1)$  and  $\psi_s(t_1)$  are accordingly the terminal conditions.

The requirements for the transient pulse pattern include the following: First, the transient pattern is required to be optimal in the sense that it minimizes the current and/or torque THD. It is also conceivable that the pulse pattern minimizes the switching losses of the power converter switches, e.g. by penalizing commutation angles that occur at high currents. Next, excessive excursions of the stator flux and thus of the stator currents are to be avoided to prevent over-current conditions. Finally, the torque and the stator flux magnitude are to be controlled around their references—at steady-state operating conditions as well as during transients.

##### B. Principle of Model Predictive Pulse Pattern Control

The above stated control problem can be formulated as a constrained optimal control problem with a so-called receding horizon policy or, equivalently, as a model predictive control (MPC) problem [13]. The key idea is to associate the prediction horizon with the time interval  $T_p = t_1 - t_0$ , and to drive the stator flux vector over this horizon to its desired position, thus correcting the stator flux error. This is enforced by adding a terminal equality constraint on the state vector. From the end of the horizon onwards, steady-state operation is assumed. In particular, the controller *assumes* that from  $t_1$  onwards the original, i.e. the *steady-state* pulse pattern, will be applied. It is crucial to note, however, that due to the receding horizon policy highlighted in the introduction and in Fig. 2, the steady-state OPP will *never* be applied. Instead, at every time-step,

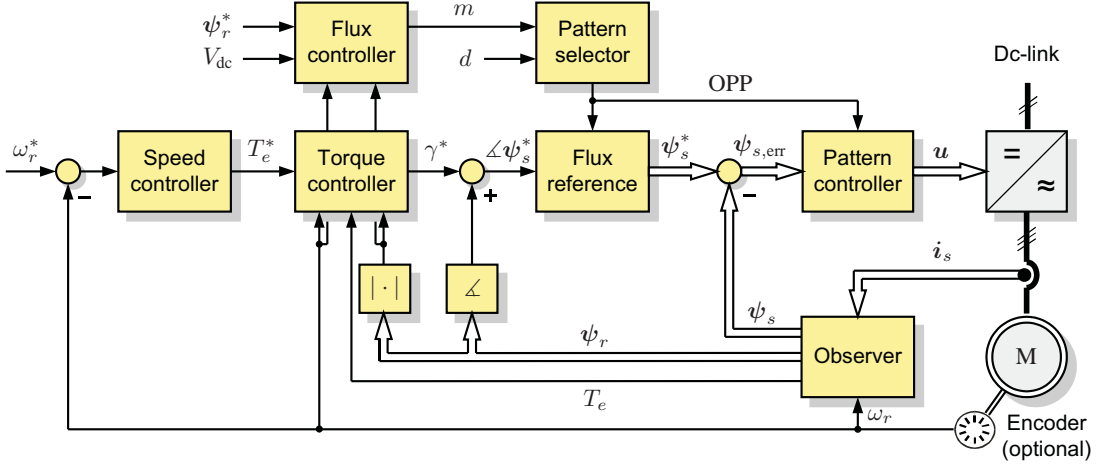


Fig. 7: Block diagram of the model predictive pulse pattern control (MP<sup>3</sup>C) scheme

the first part of the modified OPP, i.e. the pattern over the sampling interval  $T_s$ , will be applied to the drive system.

Under steady-state operating conditions, the stator flux error is small, typically amounting to one to two percent of the nominal flux magnitude. Therefore, only small corrections of the switching instants are required to remove the flux error over the horizon. As a result, the steady-state OPP can be used as a baseline pattern when deriving the transient pulse pattern. This greatly simplifies the control problem at hand, since re-optimizing the OPP around its optimum is significantly less computationally demanding than computing an entirely new transient pulse pattern from scratch.

The control objective is then to regulate the stator flux vector along its given reference trajectory in stationary coordinates, by modifying the switching instants of the OPP within the horizon as little as possible. As an example, consider phase  $a$ . According to (2), shifting the switching transition by the scalar time  $\Delta t_a$  changes the phase  $a$  stator flux by

$$\Delta\psi_{sa}(\Delta t_a) = -\frac{V_{dc}}{2}\Delta u_a\Delta t_a, \quad (3)$$

where,  $\Delta u_a = u_a(t_a^*) - u_a(t_a^* - dt)$  denotes the switching transition in phase  $a$ , with  $\Delta u_a \in \{-1, 1\}$ . The nominal switching time is given by  $t_a^*$  and  $dt$  is an infinitesimally small time step. All variables are given in per unit.

An example is shown in Fig. 6. Delaying the negative switching transition  $\Delta u_a = -1$  by  $\Delta t_a$  increases the volt-seconds and thus the stator flux in this phase. Advancing the switching event has the opposite effect, i.e. it decreases the flux amplitude in the direction of phase  $a$ . The same holds for phases  $b$  and  $c$ .

Compensation of the flux error vector in real time by modifying the switching instants of the OPP, results in fast closed-loop control. We refer to this control concept as model predictive pulse pattern control (MP<sup>3</sup>C). The internal model of this controller is based on three integrators of the form (3), one for each phase.

### C. Optimality

It is important to point out that, as indicated above, optimality, i.e. minimal current THD, is achieved when the reference stator flux trajectory is accurately tracked. Optimality is thus defined in terms of the reference flux trajectory rather than in terms of the steady-state voltage waveform. These two terms coincide only at steady-state under ideal conditions. Optimality can also be achieved for quasi steady-state conditions, by ensuring that the reference flux trajectory is closely tracked.

The following scenarios typically lead to large transients: the application of large torque steps, the switching between pulse patterns of different pulse numbers, and the shifting of operating points across discontinuities in the switching angles. In all three cases, the stator flux error tends to be large and significant corrections of the switching instants are mandatory. As a result, the transient pulse pattern obtained by re-optimizing around the existing OPP might be suboptimal. However, the notion of harmonic distortion, which is based on the frequency analysis, is not meaningful during such transients. Therefore, rather than focusing on a minimal current THD, during transients the controller aims at achieving a very fast dynamic response by rapidly tracking the new stator flux reference trajectory.

### D. Proposed MP<sup>3</sup>C Algorithm

The proposed MP<sup>3</sup>C algorithm is shown in the block diagram in Fig. 7. It operates in the discrete time domain and is activated at equally spaced time-instants  $kT_s$ , with  $k \in \mathbb{N}$  being the discrete time-step and  $T_s$  denoting the sampling interval. The control problem is formulated and solved in stationary orthogonal coordinates. The angular electrical stator and rotor frequencies of the machine are  $\omega_s$  and  $\omega_r$ , respectively. The algorithm comprises the following six steps, which are executed at the time-instant  $kT_s$ .

**Step 1.** Estimate the stator and rotor flux vectors in the stationary reference frame. This yields  $\psi_s = [\psi_{s\alpha} \ \psi_{s\beta}]^T$  and  $\psi_r = [\psi_{r\alpha} \ \psi_{r\beta}]^T$ . Let  $\angle\psi$  denote the angular position of a flux vector and  $|\psi|$  its magnitude.

Compensate for the delay introduced by the controller computation time by rotating the estimated stator and rotor flux vectors by  $\omega_s T_s$  forward in time, i.e.  $\angle \psi_s = \angle \psi_s + \omega_s T_s$  and accordingly for the rotor flux.

**Step 2.** Compute the reference of the stator flux vector  $\psi_s^*$ . Recall that the electromagnetic torque  $T_e$  produced by the machine can be written as  $T_e = k_r |\psi_s| |\psi_r| \sin(\gamma)$ , where  $k_r$  is the rotor coupling factor, and  $\gamma$  is the angle between the stator and the rotor flux vectors. When the machine is fully magnetized, the magnitude of the reference flux vector is equal to 1 pu. Then, for a given value of the rotor flux magnitude and a given torque reference, the desired angle between the stator and rotor flux vectors is

$$\gamma^* = \sin^{-1} \left( \frac{T_e^*}{k_r |\psi_r|} \right). \quad (4)$$

The reference flux vector is then obtained by integrating the chosen nominal three-phase pulse pattern; the reference angle  $\angle \psi_r + \gamma^*$  constitutes the upper limit of the integral. The resulting instantaneous reference flux vector has, in general, a magnitude and angle that slightly differ from their respective values on the unitary circle, Fig. 8. The vector diagram in this figure provides a graphical summary of the derivation of the reference flux vector.

**Step 3.** Compute the stator flux error, which is the difference between the reference and the estimated stator flux vector

$$\psi_{s,\text{err}} = \psi_s^* - \psi_s. \quad (5)$$

It is evident that this error can be directly calculated—neither the fundamental component nor the harmonic content of the stator flux need to be estimated for this. This is in stark contrast to state-of-the-art techniques [9], [10] that require an estimation of the *fundamental* flux component to evaluate the fundamental component of the stator voltages at the machine terminals. The latter quantity is then employed to derive the reference voltage vector  $u^*$ , which allows perpetuation of a desired operating point; this permits near-steady-state operation of the modulator—a requirement for employing OPPs even when the drive is in dynamic condition. Our proposed method treats the flux error (5) as a unique quantity that encompasses both (i) the harmonic flux error  $\psi_{\text{err},h}$ , which describes the deviation of the stator flux from the target flux trajectory due to excursions of the harmonic content at quasi steady-state operation, and (ii) the fundamental flux error  $\psi_{\text{err},1}$ , which is non-zero when the operating condition changes (e.g. due to step changes of the load torque or changes in the angular velocity of the machine).

**Step 4.** This step comprises the actual pulse pattern controller. The MP<sup>3</sup>C control problem can be formulated as an optimization problem with a quadratic objective function and linear constraints, a so called quadratic program (QP). The terminal equality constraint is relaxed, by replacing it by a large penalty on any uncompensated flux error. Doing so avoids numerical difficulties [12]. The objective function penalizes both the uncorrected flux error (the controlled variable) and the changes of the switching instants (the manipulated

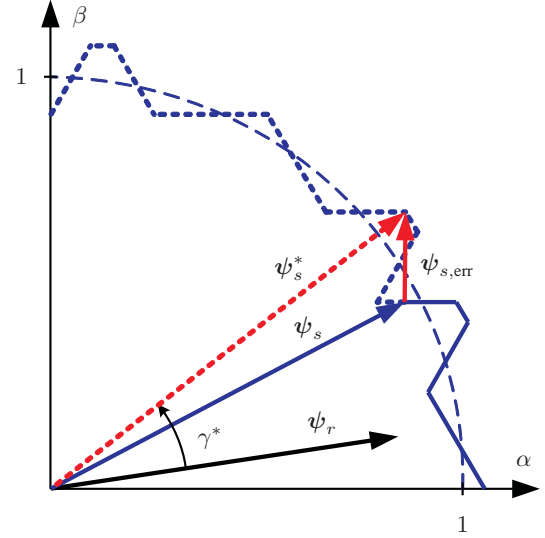


Fig. 8: Actual stator flux vector  $\psi_s$ , rotor flux vector  $\psi_r$ , reference flux vector  $\psi_s^*$  and stator flux error  $\psi_{s,\text{err}}$  in the stationary coordinates

variable)<sup>1</sup>, using the weight  $q$ , which is very small. Constraints on the switching instants ensure that the correct sequence of switching transitions is kept and that transitions are not moved into the past. Specifically, the QP is formulated as

$$\min_{\Delta t} \underbrace{(|\psi_{s,\text{err}} - \psi_{s,\text{corr}}(\Delta t)|^2 + q \Delta t^T \Delta t)}_{J(\Delta t)} \quad (6a)$$

$$\text{s. t. } kT_s \leq t_{a1} \leq t_{a2} \leq \dots \leq t_{an_a} \leq t_{a(n_a+1)}^* \quad (6b)$$

$$kT_s \leq t_{b1} \leq t_{b2} \leq \dots \leq t_{bn_b} \leq t_{b(n_b+1)}^* \quad (6c)$$

$$kT_s \leq t_{c1} \leq t_{c2} \leq \dots \leq t_{cn_c} \leq t_{c(n_c+1)}^* \quad (6d)$$

Again,  $\psi_{s,\text{err}}$  is the stator flux error in stationary coordinates ( $\alpha\beta$ ),  $\psi_{s,\text{corr}}(\Delta t)$  is the correction of the stator flux, and  $\Delta t = [\Delta t_{a1} \ \Delta t_{a2} \ \dots \ \Delta t_{an_a} \ \Delta t_{b1} \ \dots \ \Delta t_{bn_b} \ \Delta t_{c1} \ \dots \ \Delta t_{cn_c}]^T$  denotes the vector of switching instant corrections. For phase  $a$ , for example, the correction of the  $i$ -th transition time is given by  $\Delta t_{ai} = t_{ai} - t_{ai}^*$ , where  $t_{ai}^*$  denotes the nominal switching instant of the  $i$ -th transition  $\Delta u_{ai}$ . Again, the latter is defined as  $\Delta u_{ai} = u_a(t_{ai}^*) - u_a(t_{ai} - dt)$  with  $dt$  being an infinitesimally small time step. Moreover,  $n_a$  denotes the number of switching transitions in phase  $a$  that are within the prediction horizon, and  $t_{a(n_a+1)}^*$  refers to the first nominal switching transition beyond the horizon. The quantities for phases  $b$  and  $c$  are defined accordingly.

<sup>1</sup>The penalty on the manipulated variable is a further difference to state-of-the-art methods, which typically only penalize the controlled variable [7], [9]. Here, it is proposed to also minimize the *change* of the switching instants so that the pattern controller in Fig. 7 preserves the volt-second balance of the precalculated OPP as much as possible. In this way, the controller encompasses an inherent mechanism to avoid overcompensating the flux error; this feature minimizes the interference with the optimal volt-second balance of the OPPs, thus enabling optimal operation at quasi steady-state. The dynamic performance is not compromised, if the weight  $q$  is set to a small value, putting priority on correcting the stator flux error.

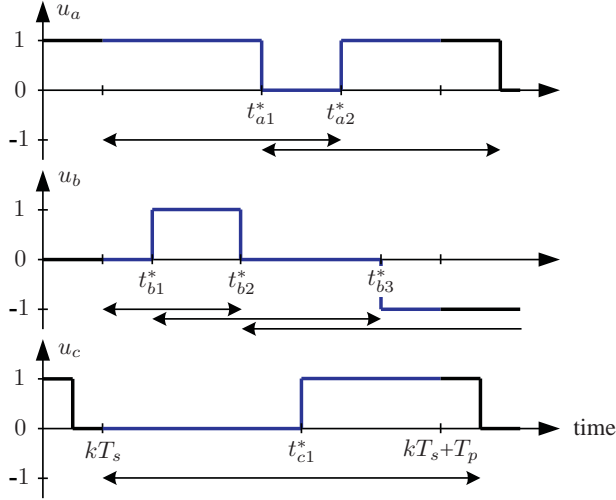


Fig. 9: Model predictive pulse pattern control (MP<sup>3</sup>C) problem for a three-phase three-level pulse pattern. Six switching transitions fall within the horizon  $T_p$ , which is of fixed length. The lower and upper bounds for the nominal switching instants are depicted by arrows

The stator flux correction is obtained by rewriting (3)

$$\psi_{s,\text{corr}}(\Delta t) = -\frac{V_{\text{dc}}}{2} \mathbf{P} \begin{bmatrix} \sum_i \Delta u_{ai} \Delta t_{ai} \\ \sum_i \Delta u_{bi} \Delta t_{bi} \\ \sum_i \Delta u_{ci} \Delta t_{ci} \end{bmatrix}. \quad (7)$$

The switching instants cannot be modified arbitrarily—they are constrained by the current time-instant  $kT_s$  as well as by the neighboring switching transitions in the same phase. Fig. 9 provides an example to illustrate this. The first switching transition in phase  $b$ , for example, is constrained to lie between  $kT_s$  and the nominal switching instant of the second transition in phase  $b$ ,  $t_{b2}^*$ . The second switching transition in phase  $b$  can only be delayed up to the nominal switching instant of the third transition in the same phase,  $t_{b3}^*$ . In this example, the number of transitions that fall within the prediction horizon are  $n_a = 2$ ,  $n_b = 3$  and  $n_c = 1$ . Note that the transitions in a given phase are modified independently from those in the other phases.

The horizon length  $T_p$  is a design parameter. If required,  $T_p$  is increased so as to ensure that switching transitions in at least two phases fall within the horizon. Consider again Fig. 9. In case  $T_p$  is smaller than  $t_{a1}^* - kT_s$ , it is increased to this value.

**Step 5.** Remove switching transitions from the QP that will occur within the sampling interval. This can be accomplished by updating a pointer to the look-up table that stores the switching angles of the OPP and the respective three-phase potential values.

**Step 6.** Derive the switching commands over the sampling interval, i.e. the switching instants and the associated switch positions. The switching commands are sent to the gate units of the semiconductor switches in the inverter.

To reiterate, even though a sequence of switch positions is planned over a long prediction horizon, only the switching

sequence over the sampling interval is executed. The predictions are recomputed at the next sampling interval using new measurements; a shifted—and if necessary revised—sequence of switch positions is derived. This is referred to as the receding horizon policy, see Fig. 2, which provides feedback and makes MP<sup>3</sup>C robust to the flux estimation errors and non-idealities mentioned earlier. Longer horizons reduce the controller sensitivity to flux estimation errors, as will be shown in Sect. VI-B. As a result, the steady-state current distortions tend to be lower, when compared with an overly aggressive controller, i.e. a controller that operates with a very short prediction horizon and does not penalize the corrective action ( $q = 0$ ).

### E. Additional Control Loops

The inner MP<sup>3</sup>C control loop described above is augmented by two outer control loops, as shown in Fig. 7. The first loop regulates the torque by adjusting the reference angle between the stator and the rotor flux vectors. The second loop regulates the stator flux magnitude by adjusting the modulation index. The slow stator flux controller uses information from the inner loop of MP<sup>3</sup>C to adjust the modulation index—specifically, the volt-second correction or the effective modulation index.

The OPP method is conceptually applicable to the whole speed range. Specifically, OPPs can inherently reach six-step operation at the upper end of the modulation index. At the lower end, however, OPPs are restricted by the following factors: (i) the pulse number  $d$  increases at low modulation indices and low frequencies, making the computations to derive OPPs more challenging; and (ii) the advantage of OPPs over carrier-based PWM becomes insignificant in terms of the current THD. Therefore, the standard practice is to switch to carrier-based PWM at low modulation index (e.g. below 0.3 pu). This issue is explained in detail in [10].

## V. COMPUTATIONAL ASPECTS

### A. Active Set Method to Solve the QP

The QP formulated in Step 4 can be solved efficiently by adopting the so called active set method for quadratic programming. This is a standard approach to solve QPs of small to medium scale. The active set method is described in detail for example in [16, Sect. 16.4].

We start by computing the unconstrained solution, i.e. we minimize (6a), while neglecting the timing constraints (6b)–(6d). We also recall that the step size of all switching transitions is  $\pm 1$ , i.e.  $|\Delta u_{ai}| = 1$ , and accordingly for phases  $b$  and  $c$ . It is obvious that—in the unconstrained case—the resulting modifications of the switching instants are the same per phase. We can thus define  $\delta_a = \frac{1}{3} \frac{V_{\text{dc}}}{2} \Delta t_{ai}$  for phase  $a$ , with  $\delta_a$  denoting the scaled volt-second modification for the transitions in phase  $a$ . The per-phase variables defined above can be aggregated to the three-phase vectors  $\boldsymbol{\delta} = [\delta_a \ \delta_b \ \delta_c]^T$  and  $\mathbf{n} = [n_a \ n_b \ n_c]^T$ . Recall that  $n_a$  denotes the number of switching transitions in phase  $a$ , with  $n_b$  and  $n_c$  defined accordingly for phases  $b$  and  $c$ . As an example for the latter, refer to Fig. 9, which corresponds to  $\mathbf{n} = [2 \ 3 \ 1]^T$ .

Introducing the constant  $\varrho = \frac{1}{2}q/(\frac{1}{3}\frac{V_{dc}}{2})^2$ , we can rewrite  $J$  in (6a) as

$$J(\delta) = |\psi_{s, \text{err}} - \psi_{s, \text{corr}}(\delta)|^2 + 2\varrho(n_a\delta_a^2 + n_b\delta_b^2 + n_c\delta_c^2) \quad (8)$$

and (7) as  $\psi_{s, \text{corr}}(\delta) = -3\mathbf{P}\mathbf{n}^T\delta$ . Setting  $\nabla J(\delta)$  to zero yields the unconstrained minimum

$$\delta = -\mathbf{M}^{-1}\mathbf{P}^{-1}\psi_{s, \text{err}} \quad (9)$$

with

$$\mathbf{M} = \begin{bmatrix} 2n_a + \varrho & -n_b & -n_c \\ -n_a & 2n_b + \varrho & -n_c \\ -n_a & -n_b & 2n_c + \varrho \end{bmatrix}. \quad (10)$$

The expression  $\mathbf{M}^{-1}\mathbf{P}^{-1}$  can be derived algebraically and does not need to be computed in real time.

The tailored active set method to solve the QP (6) involves several iterations of the following three steps.

**Step 1.** Compute the number of switching transitions  $n$  per phase that fall within the horizon.

**Step 2.** Neglect the timing constraints and compute the unconstrained volt-second corrections  $\delta$  per phase. Convert these into unconstrained switching instants, taking the sign of the switching transition into account. For the  $i$ -th transition in phase  $a$ , this implies  $t_{ai} = t_{ai}^* + 3\frac{2}{V_{dc}}\frac{\delta_a}{\Delta u_{ai}}$ . The unconstrained switching instants in phases  $b$  and  $c$  are defined accordingly.

**Step 3.** Impose the timing constraints (6b)–(6d) by determining the switching instants that violate one or more of the constraints (the so-called *active constraints*). For the active constraints, perform the following operations:

- 1) Limit the unconstrained switching instants by imposing the constraints. This yields the final solution for these switching instants.
- 2) Remove these switching instants and their associated switching transitions from the optimization problem and reduce  $n$  accordingly.
- 3) Compute the flux correction that results from these modified switching instants and update the remaining (as yet uncorrected) flux error accordingly.

Iterate over Steps 2 and 3 again until the solution remains unchanged. In general, two iterations suffice.

This procedure is computationally simple. Most importantly, the computational complexity is effectively independent of the number of considered switching transitions and thus of the length of the horizon. Specifically, the dimension of the matrix  $\mathbf{M}^{-1}\mathbf{P}^{-1}$  is always  $3 \times 2$ . Since the offline computed OPP always has switching transitions of step-size one, the above outlined active set method yields the same result as the QP formulation (6). Small differences would occur, if some transitions had step-sizes greater than one. In the remainder of the paper, we refer to this as *MP<sup>3</sup>C based on QP*, or simply as the *QP method*.

### B. MP<sup>3</sup>C based on Deadbeat Control

Another alternative is to set the weight  $q$  in (6a) to zero. As a result, the degree by which the switching instants are modified is not penalized. The horizon is kept as short as

Induction motor	Voltage	3300 V	$r_s$	0.0108 pu
	Current	356 A	$r_r$	0.0091 pu
	Real power	1.587 MW	$x_{ls}$	0.1493 pu
	Apparent power	2.035 MVA	$x_{lr}$	0.1104 pu
	Frequency	50 Hz	$x_m$	2.3489 pu
	Rotational speed	596 rpm		
Inverter			$V_{dc}$	1.930 pu
			$x_c$	11.769 pu

TABLE I: Rated values (left) and parameters (right) of the drive

possible. Specifically, the horizon is redefined as the minimum time interval starting at the current time instant such that at least two phases exhibit switching transitions. This leads to a pulse pattern controller with deadbeat (DB) characteristic. The control algorithm is computationally and conceptually very simple, as summarized in the following.

**Step 1.** Determine the two phases that have the next scheduled switching transitions. We refer to those as the *active* phases, which are always pairs, i.e.  $ab$ ,  $bc$  or  $ac$ . This yields the length of the horizon  $T_p$ , which is of variable length for the DB controller. Determine all switching transitions within the horizon. In Fig. 9, for example, phases  $a$  and  $b$  have the next switching transitions and are thus the active phases. Their nominal switching instants are  $t_{b1}^*$ ,  $t_{b2}^*$  and  $t_{a1}^*$ . The horizon thus spans the time interval from  $kT_s$  to  $t_{a1}^*$ .

**Step 2.** Translate the flux error from  $\alpha\beta$  to  $abc$ , by mapping it into the two active phases. The flux error of the third phase is zero. For the example above, with the active phases  $a$  and  $b$ , the mapping is given by  $\psi_{s, abc, \text{err}} = \mathbf{P}_{ab}^{-1}\psi_{s, \text{err}}$  with

$$\mathbf{P}_{ab}^{-1} = \begin{bmatrix} \frac{3}{2} & \frac{\sqrt{3}}{2} \\ 0 & \sqrt{3} \\ 0 & 0 \end{bmatrix}. \quad (11)$$

**Step 3.** Compute the required modification of the switching instants in  $abc$ , given by  $\Delta t_{\text{req}} = \psi_{s, abc, \text{err}}/(V_{dc}/2)$ .

**Step 4.** Go through all switching transitions of the first active phase  $x$ , with  $x \in \{a, b, c\}$ . For the  $i$ -th switching transition in this phase with the nominal switching instant  $t_{xi}^*$  and the switching transition  $\Delta u_{xi}$ , perform the following operations:

- Compute in a DB fashion the desired modification  $\Delta t_{xi} = \Delta t_{x, \text{req}}/(-\Delta u_{xi})$ .
- Modify the switching instant to  $t_{xi} = t_{xi}^* + \Delta t_{xi}$ .
- Constrain  $t_{xi}$  by imposing the respective timing constraints on the switching instant.
- Update the phase  $x$  component of the required switching instant modification, by replacing  $\Delta t_{x, \text{req}}$  with  $\Delta t_{x, \text{req}} - (t_{xi} - t_{xi}^*)(-\Delta u_{xi})$ .

Repeat the above procedure for the second active phase.

Note that  $t_{xi} - t_{xi}^*$  equals the desired modification  $\Delta t_{xi}$  only when the associated constraints are not active. Since the DB controller aims at removing the stator flux error as quickly as possible and since corrections in the switching instants are not penalized, the DB controller tends to be very fast and aggressive. Yet, there is no guarantee that the flux error is

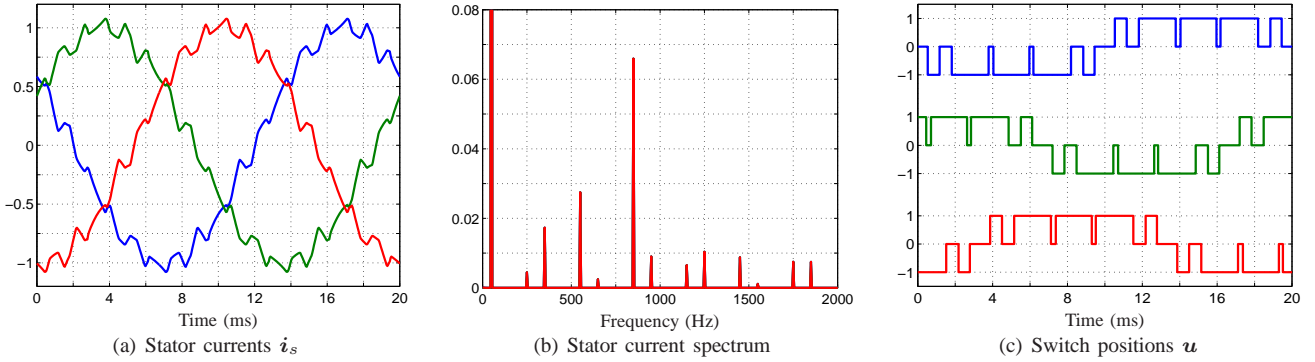


Fig. 10: Space vector modulation (SVM) at nominal speed and full torque with the carrier frequency  $f_c = 450$  Hz. The modulation index is  $m = 0.82$ . The stator currents and the switch positions are shown versus the time-axis in ms, while the stator current spectrum is depicted versus the frequency axis in Hz. All quantities are given in pu

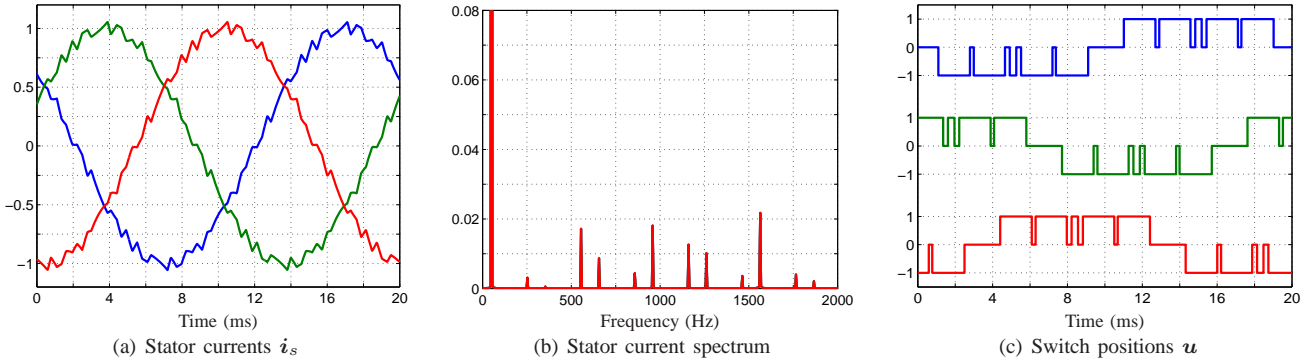


Fig. 11: Model predictive pulse pattern control (MP<sup>3</sup>C) with the pulse number  $d = 5$ . The operating point, the switching frequency, the plots and their scaling are the same as in Fig. 10 to facilitate a direct comparison

fully removed within the horizon, since the constraints on the switching instants have to be respected<sup>2</sup>.

### C. Computational Requirements

Another major advantage of the proposed MP<sup>3</sup>C scheme relates to the ease of implementation, specifically to the number of computations to be performed on the controller hardware within the sampling interval. In general, the computational burden is often quite pronounced for MPC, requiring a powerful control platform to achieve the high steady-state and dynamic performance demonstrated in [17]–[19]. For the proposed control scheme, however, by pre-computing optimized pulse patterns, the majority of the computations is moved offline at the expense of an increased memory requirement to store these patterns. During runtime, the pulse pattern is modified by the controller so as to compensate for non-idealities and to achieve fast control during transients.

Nevertheless, in the low-frequency operating range, field-oriented control and carrier-based PWM are required, impos-

<sup>2</sup>The DB version of MP<sup>3</sup>C might appear to bear some similarities with state-of-the-art methods [9], [10]. These, however, typically sample the flux error every  $500 \mu\text{s}$ , map the  $\alpha\beta$  flux error into all three phases using (1), modify the switching instants within these  $500 \mu\text{s}$  and send the modified pulse pattern sequence over the whole  $500 \mu\text{s}$  to the inverter. In contrast to that, the proposed DB controller adopts the receding horizon policy—the gating commands are set over the sampling interval, which typically encompasses  $25 \mu\text{s}$ , while the prediction horizon is usually in the range of 0.5 to 1 ms.

ing additional requirements on the control hardware. Specifically, the trajectory controller with OPPs and the field-oriented controller with carrier-based PWM co-exist on the same hardware. Since the effort to modify the pre-computed OPPs is roughly the same as the effort to establish control by field orientation, the maximal computation time is well below  $25 \mu\text{s}$  and thus below the sampling period.

## VI. PERFORMANCE EVALUATION

As a case study, consider a three-level NPC voltage source inverter driving an induction machine with a constant mechanical load, as shown in Fig. 1. A 3.3 kV and 50 Hz squirrel-cage induction machine rated at 2 MVA with a total leakage inductance of 0.25 pu is used as an example of a typical medium-voltage induction machine. The dc-link voltage is  $V_{dc} = 5.2$  kV and the modulation index (as defined in [7]) is  $m = 0.82$  for all cases. The detailed parameters of the machine and the inverter are summarized in Table I. The per unit system is established using the base quantities  $V_B = \sqrt{2/3}V_{rat} = 2694$  V,  $I_B = \sqrt{2}I_{rat} = 503.5$  A and  $f_B = f_{rat} = 50$  Hz.

### A. Steady-State Operation under Nominal Conditions

At nominal speed and rated torque, closed-loop simulations were run to evaluate the performance of MP<sup>3</sup>C under steady-state operating conditions. The key performance criteria are

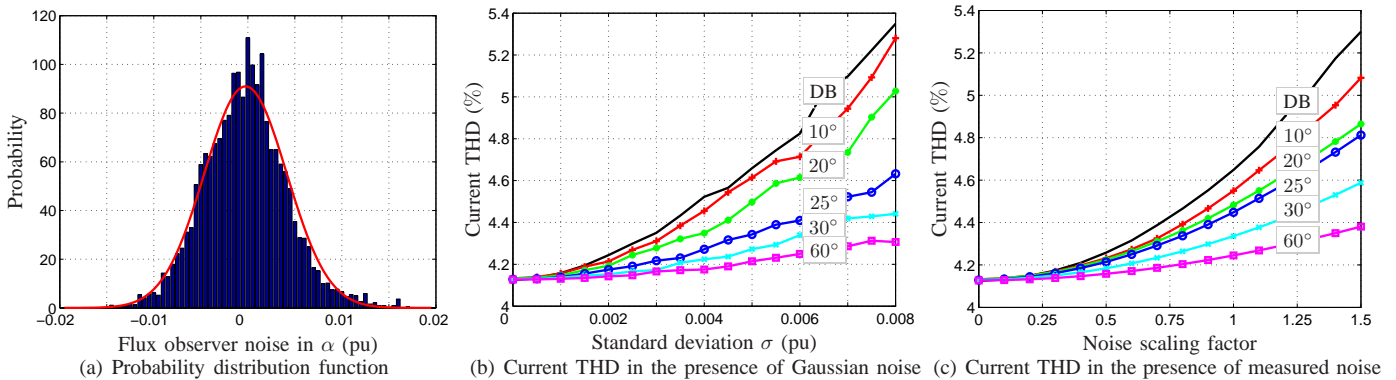


Fig. 12: Influence of flux observer noise on the closed-loop performance of MP<sup>3</sup>C. Fig. (a) shows the probability distribution function of the noise measured in the medium-voltage lab. Figs. (b) and (c) depict the current THD as a function of the noise level for Gaussian and measured noise, respectively. The straight (black) line refers to DB control, whereas the (colored) lines with markers refer to QP control with different horizon lengths, namely  $\theta_p = 10^\circ, 20^\circ, 25^\circ, 30^\circ, 60^\circ$ . The pulse number is  $d = 5$ , and the operating point is at nominal speed and full torque, as in Fig. 11

Control scheme	Control setting	$f_{sw}$ [Hz]	$I_{s,THD}$ [%]	$T_{e,THD}$ [%]	$I_{s,THD}$ [%]	$T_{e,THD}$ [%]
CB	$f_c = 250$ Hz	150	16.1	11.0	100	100
SVM	$f_c = 250$ Hz	150	15.5	9.83	96.8	89.6
MP <sup>3</sup> C	$d = 3$	150	7.36	6.62	45.9	60.3
CB	$f_c = 450$ Hz	250	7.94	5.79	100	100
SVM	$f_c = 450$ Hz	250	7.71	5.35	97.1	92.4
MP <sup>3</sup> C	$d = 5$	250	4.13	3.41	52.0	58.9
CB	$f_c = 750$ Hz	400	4.68	3.41	100	100
SVM	$f_c = 750$ Hz	400	4.52	3.06	96.6	89.7
MP <sup>3</sup> C	$d = 8$	400	3.63	2.88	77.6	84.5

TABLE II: Comparison of MP<sup>3</sup>C with CB-PWM and SVM in terms of the switching frequency  $f_{sw}$ , the current THD  $I_{s,THD}$  and the torque THD  $T_{e,THD}$ . The center section shows absolute values, while the values in the right section are relative, using CB-PWM as a baseline. The pulse number is given by  $d$  and the carrier frequency by  $f_c$ . In all cases the modulation index is  $m = 0.82$ . The operating point is at nominal speed and rated torque, and nominal conditions are assumed, i.e. the stator flux observations are not affected by noise and the machine parameters are precisely known

the harmonic distortions of the current and torque for a given switching frequency. The simulated MP<sup>3</sup>C is based on the DB controller, which at steady-state yields nearly identical results to the QP version. OPPs were calculated offline with various pulse numbers, according to Sect. III-A. MP<sup>3</sup>C is compared with two commonly used modulation methods—carrier-based pulse width modulation (CB-PWM) and space vector modulation (SVM). Specifically, a three-level regular sampled PWM is implemented with two in-phase triangular carriers, so-called phase disposition (PD). It is generally accepted that for multi-level inverters, carrier-based PWM with PD results in the lowest harmonic distortion. In accordance with common practise, the reference signals are generated by adding a one sixth third harmonic to the modulating reference signals to boost the differential-mode voltage. The SVM is obtained by adopting the approach proposed in [20]: A common mode voltage, which is of the min/max type plus a modulus operation, is added to the reference voltage.

The data in Table II show that for low switching frequencies of a few hundred Hertz, as typically used in MV drives, MP<sup>3</sup>C

effectively halves the current distortions for the same switching frequency, when compared to CB-PWM or SVM. It can also be seen that the THD performances for CB-PWM or SVM are quite similar. The CB-PWM and SVM values come closer to the MP<sup>3</sup>C results as the switching frequency increases—although MP<sup>3</sup>C is still considerably better than both PWM methods over the range displayed.

The current waveform and spectrum along with the phase leg switch positions are shown for SVM and MP<sup>3</sup>C DB modulation respectively in Figs. 10 and 11. These figures refer to the fifth and sixth row in the table, i.e. the middle switching frequency considered in the comparison. From the current waveforms it is readily apparent that MP<sup>3</sup>C produces a much lower current ripple. Correspondingly, the harmonic components of the MP<sup>3</sup>C current spectrum are much reduced, particularly regarding the harmonics around  $f_c$  and the 17th harmonic.

### B. Steady-State Operation with Flux Observer Noise

MP<sup>3</sup>C requires an accurate estimate of the stator flux vector. For this, a flux observer is used, as shown in Fig. 7, which is typically affected by noise. This section investigates the impact such observer noise has on the closed-loop performance of MP<sup>3</sup>C, particularly with regards to the current THD.

For this, MP<sup>3</sup>C was run at nominal speed and torque under steady-state operating conditions on a 1 MVA medium-voltage drive in the laboratory. The evolution of the stator flux vector was measured along with the one of the stator flux reference vector. The difference between the two stator flux vectors was defined in (5) as the stator flux error  $\psi_{s,err}$ . At steady-state operation, MP<sup>3</sup>C removes the flux error almost completely—the residual error typically accounts for less than one percent of the nominal flux magnitude. This residual error is dominated by noise from the flux observer. In the following, we therefore refer to  $\psi_{s,err}$  as the flux observer noise, which includes noise sources in the path of the stator flux estimation, such as drift in the current measurement and ripple of the angular velocity signal: both are inputs to the flux observer,

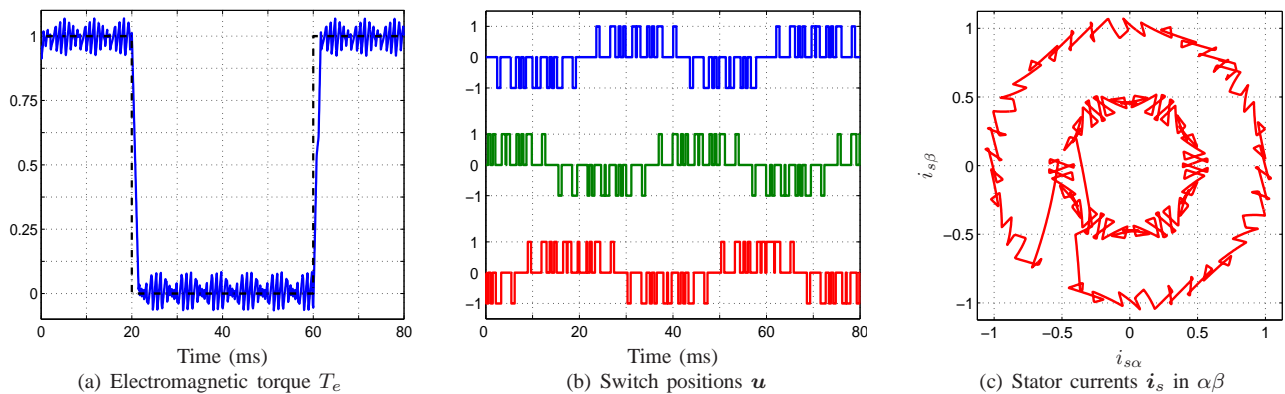


Fig. 13: DB MP<sup>3</sup>C at 50% speed with an OPP of pulse number  $d = 10$  ( $f_{sw} = 250$  Hz) and steps in the torque reference. The torque and the switch positions are shown versus the time-axis in ms. The stator currents are depicted in stationary orthogonal coordinates. All quantities are given in pu

Fig. 7. Uncompensated non-idealities of the power inverter also contribute to the residual noise.

Fig. 12(a) shows the probability distribution function (PDF) of the flux observer noise in the  $\alpha$ -axis, with the noise in the  $\beta$ -axis being very similar. Note that the integral of the PDF is one. The noise can be well approximated as Gaussian noise with zero mean value and the standard deviation  $\sigma = 0.0044$  pu, as shown by the red line in Fig. 12(a). However, the noise exhibits a certain degree of auto-correlation, implying that the noise amplitude at time-instant  $k$  somewhat depends on the noise amplitude at the previous time-instant  $k - 1$ . This auto-correlation is not captured by the Gaussian noise. In the following, we distinguish between *Gaussian noise* and *measured noise*. The Gaussian noise is characterized by a given standard deviation and exhibits no auto-correlation. The measured noise is the measured  $\psi_{s,err}$ , whose PDF is effectively Gaussian, but features a non-zero auto-correlation.

Before proceeding, we define the (angular) prediction horizon  $\theta_p = 360 f_B \omega_r \cdot T_p$  in degree, which refers to the angular spread MP<sup>3</sup>C looks into the future, while the (time) prediction horizon  $T_p$  is given in seconds.

Using the same setting as in the previous section (nominal speed, full torque,  $d = 5$ ), the impact of Gaussian observer noise on the current THD is shown in Fig. 12(b). Without noise the current THD is 4.13%, c.f. also to the sixth row in Table II. For DB MP<sup>3</sup>C control and  $\sigma = 0.0044$  pu, the current THD deteriorates by 10% to 4.57%. When using QP MP<sup>3</sup>C, the deterioration due to noise can be reduced as the horizon length is increased. For the long horizon  $\theta_p = 60^\circ$  this deterioration is effectively avoided altogether—the current THD is 4.19%, which is equivalent to a deterioration of only 1.5%. Note that at nominal speed  $\theta_p = 60^\circ$  is equivalent to  $T_p = 3.33$  ms.

The impact of the measured noise on the current THD is similar, as shown in Fig. 12(c). In this, the noise scaling factor denotes a factor, with which the amplitude of the measured noise is multiplied, allowing us to study the effect of different noise intensities. When the scaling factor is one, DB control results in a current THD of 4.65%, which is 13% worse than

the nominal case. For QP MP<sup>3</sup>C with  $\theta_p = 60^\circ$  the current THD can be brought down to 4.24%, which implies a 2.7% deterioration.

In Figs. 12(b) and 12(c), it can be seen that for QP control the resilience to flux observer noise changes significantly when increasing the (angular) prediction horizon from  $\theta_p = 20^\circ$  to  $\theta_p = 30^\circ$ . The reason for this is that for  $\theta_p = 20^\circ$ , in 14% of the time-steps, the prediction horizon captures switching transitions in only two phases, i.e.  $T_p < t_{c1}^* - kT_s$  in Fig. 9. For  $\theta_p = 30^\circ$  the horizon is long enough to always include switching transitions in all three phases, i.e.  $T_p \geq t_{c1}^* - kT_s$  in Fig. 9.

Only two phases are required to decompose the flux error in its components and to compensate them. However, the flux error compensation is less vulnerable to noise when switching transitions in all three phases are available, because in this case smaller modifications of the switching time instants are required. The intuitive assumption that a longer prediction horizon makes the control scheme more robust is thus verified.

Summing up, on the one hand, the DB version is affected by flux observer noise, which is a common characteristic of such an aggressive control scheme. The QP approach, on the other hand, is less susceptible to noise, particularly for long horizons, since the controller carefully weighs in the objective of removing the flux error within the horizon versus the penalty on modifying the switching transitions. This is a fundamental characteristic of so called optimal control schemes, such as QP MP<sup>3</sup>C, which are based on the trade-off between good tracking performance and low control effort. In this case, this trade-off is determined by the length of the horizon. The penalty  $q$  has only a minor effect, in that it decides on the trade-off between control effort and the terminal soft constraint.

Above we assumed  $\sigma = 0.0044$  pu and the noise scaling factor of one to be representative for flux observer noise in a real-world medium-voltage drive setting. This assumption might be pessimistic, since the recorded noise also includes uncompensated stator flux errors. The real observer noise is thus probably one third smaller. The corresponding deteriora-

Control scheme	$R_s$ [%]	$R_r$ [%]	Deviation of $T_e$ [%]	Deviation of $ \psi_s $ [%]	Deviation of $ \psi_r $ [%]
DB	75	100	0.19	0.03	0.02
DB	125	100	-0.18	-0.04	-0.02
QP	75	100	0.24	0.12	0.11
QP	125	100	-0.24	-0.12	-0.11
DB	100	75	0.13	0.00	-0.02
DB	100	125	-0.08	0.00	0.02
QP	100	75	0.42	0.06	0.03
QP	100	125	-0.36	-0.05	-0.03

TABLE III: Robustness of MP<sup>3</sup>C to machine parameter variations under steady-state operating conditions, using DB and QP control with  $\theta_p = 30^\circ$ . The deviations of the torque, stator flux and rotor flux magnitudes from their references are shown in percent, when altering the stator and rotor resistance by  $\pm 25\%$ , respectively

tion of the current THD is then 5% for DB MP<sup>3</sup>C and 1% for the QP controller with a long horizon, respectively. It can be concluded that MP<sup>3</sup>C is robust to flux observer noise.

### C. Steady-State Operation under Machine Parameter Variations

Another potential source of control performance degradation are variations in the machine parameters unaccounted for by the controller. In the following, we investigate the impact that changes in the stator and rotor resistance,  $R_s$  and  $R_r$ , have on the steady-state tracking accuracy of MP<sup>3</sup>C. As previously, operation at nominal speed and torque with an OPP with pulse number  $d = 5$  is assumed. The resistances are altered by  $\pm 25\%$ . The performance of DB MP<sup>3</sup>C is compared with the QP version with  $\theta_p = 30^\circ$  in terms of the steady-state deviation of the torque, as well as of the stator and rotor flux magnitudes from their respective references. For this, the outer flux and torque control loops, see Fig. 7, are disabled. Small steady-state errors are to be expected, particularly for the QP variety, due to MP<sup>3</sup>C lacking an integral term, which is included in PI-controllers, for example.

As shown in Table III, the steady-state errors are below 0.5% and thus barely measurable. Variations in the stator resistance are of minor importance, since the resulting voltage drop is quite small. Variations in the rotor resistance also have only a minor effect, since they merely alter the time-constant of the coupling between the stator and rotor sides. By forcing the stator flux vector along its desired trajectory, both errors can be compensated for. In general, DB MP<sup>3</sup>C performs better in the presence of machine parameter variations, which is in line with the discussion above. To compensate for these small errors, the outer loops are used, which include integral terms. These parameter variations neither have an impact on the current or torque THD, nor do they influence the resulting switching frequency.

### D. Torque Steps

The dynamic performance of MP<sup>3</sup>C during torque reference steps is investigated hereafter. At 50% speed,  $\pm 1$  pu steps on the torque reference are imposed, using an OPP with pulse

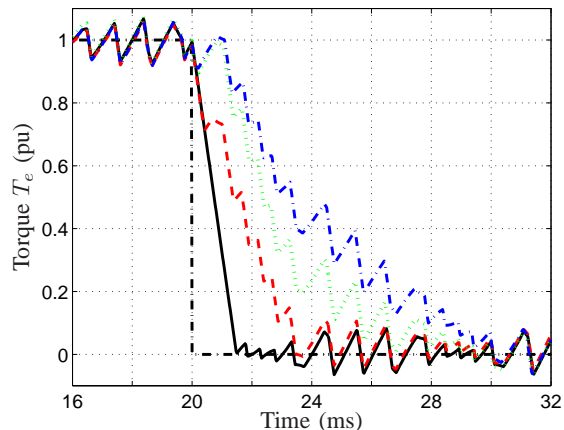


Fig. 14: Torque response to the torque step at time  $t = 20$  ms in Fig. 13. The straight (black) line refers to DB MP<sup>3</sup>C, the dashed (red) line to QP MP<sup>3</sup>C with  $\theta_p = 10^\circ$  ( $T_p = 1.11$  ms), the dotted (green) line to  $\theta_p = 30^\circ$  ( $T_p = 3.33$  ms), and the dash-dotted (blue) line corresponds to  $\theta_p = 60^\circ$  ( $T_p = 6.67$  ms)

number  $d = 10$ , which entails a switching frequency of  $f_{sw} = 250$  Hz. The transient performance of MP<sup>3</sup>C with DB control is shown in Fig. 13, with the steps in the torque reference being applied at time-instants  $t = 20$  ms and 60 ms. For DB control, the settling time is below two ms and thus similar to those for standard DB and hysteresis control schemes. Over- and undershoots are avoided, which is also evidenced by the stator current trajectory in stationary orthogonal coordinates, shown in Fig. 13(c).

In the sequel, we focus on the first torque step at  $t = 20$  ms, comparing the transient performance of DB and QP MP<sup>3</sup>C with different (angular) prediction horizons with each other. Fig. 14 shows the respective torque responses, whereas the corresponding switching sequences are shown in Fig. 15. For these figures, a time-axis zoomed in around  $t = 20$  ms is used.

When applying the torque step, the reference angle of the stator flux is to be reduced by  $13.7^\circ$ , according to (4). This is equivalent to shifting the nominal OPP by 1.52 ms forward in time. As can be seen in Fig. 13(c), the stator current's  $\alpha$ -component must be increased by almost 0.2 pu, whereas the  $\beta$ -component is to be increased by close to 0.8 pu. To achieve this, additional volt-second contributions are required—positive from phases  $a$  and  $b$ , and negative from phase  $c$ . DB control, as shown in Fig. 15(a), achieves this by removing the two negative pulses in phases  $a$  and  $b$  and by shortening the positive pulse in phase  $c$ . The resulting torque settling time is less than two ms.

QP MP<sup>3</sup>C leads to slower torque responses—for  $\theta_p = 10^\circ$  it amounts to almost 4 ms, for  $\theta_p = 30^\circ$  it is about 8 ms and for  $\theta_p = 60^\circ$  about 10 ms. As the prediction horizon is increased, the required volt-second correction is distributed over more switching transitions, as is evidenced in Figs. 15(b) and 15(c). The transition times of the pulses are modified in an effectively symmetrical manner.

In practice, most applications that demand a moderate

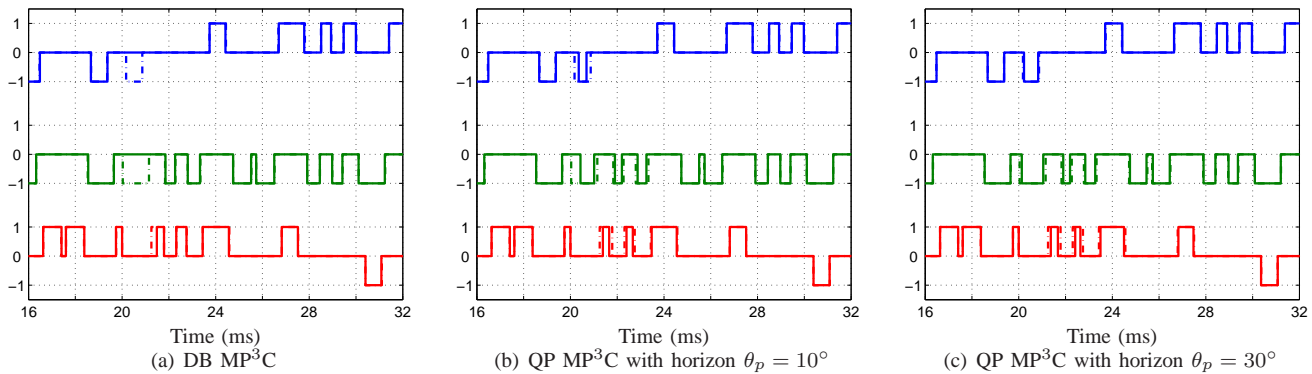


Fig. 15: Switch positions  $\mathbf{u}$  for DB and QP MP<sup>3</sup>C, corresponding to the torque step response in Fig. 14. The dash-dotted lines refer to the switching sequence of the unmodified, original OPP, whereas the straight lines correspond to the closed-loop switching sequence, modified by MP<sup>3</sup>C

dynamic performance can be served by QP MP<sup>3</sup>C. Such applications include general-purpose drives for fans and pumps, where the operating point is mostly fixed. Nowadays, drive customers demand an increased harmonic performance at steady-state—this goal is easily achieved with QP MP<sup>3</sup>C. Robustness to flux observer noise is a further advantage of QP MP<sup>3</sup>C. When a high dynamic performance is required, as in steel mill applications, switching to DB control during large transients is conceivable, so as to achieve very short response times. Moreover, variations in the machine parameters, whose impact on the steady-state performance was investigated above, have virtually no effect on the transient behavior of MP<sup>3</sup>C.

## VII. CONCLUSIONS

This paper proposed a new model predictive controller (MPC) based on optimized pulse patterns (OPPs) that resolves the classic contradiction inherent to drive control—very fast control during transients on the one hand, and optimal performance at steady-state on the other, i.e. minimal current THD for a given switching frequency. The former is typically achieved only by deadbeat control schemes and direct torque control, while the latter is in the realm of pre-calculated optimized pulse patterns. The proposed controller, MP<sup>3</sup>C, achieves both objectives, by adopting the principles of constrained optimal control and receding horizon policy. This method inherently provides robustness, while respecting the optimal volt-second balance of the OPPs under quasi steady-state and dynamic conditions. The result are very fast current and torque responses during transients and very low harmonic distortion levels per switching frequency at steady-state operating conditions.

## REFERENCES

- [1] H. S. Patel and R. G. Hoft. Generalized techniques of harmonic elimination and voltage control in thyristor inverters: Part I—Harmonic elimination. *IEEE Trans. Ind. Appl.*, 9(3):310–317, May/June. 1973.
- [2] G. S. Buja. Optimum output waveforms in PWM inverters. *IEEE Trans. Ind. Appl.*, 16(6):830–836, Nov./Dec. 1980.
- [3] T. Boller, J. Holtz, and A.K. Rathore. Optimal pulsewidth modulation of a dual three-level inverter system operated from a single dc link. In *Proc. IEEE Energy Convers. Congr. Expo.*, pages 3406–3410, Phoenix, AZ, USA, Sep. 2011.
- [4] J. Holtz and B. Beyer. Fast current trajectory tracking control based on synchronous optimal pulsewidth modulation. *IEEE Trans. Ind. Appl.*, 31(5):1110–1120, Sep./Oct. 1995.
- [5] J. Holtz and B. Beyer. The trajectory tracking approach—A new method for minimum distortion PWM in dynamic high-power drives. *IEEE Trans. Ind. Appl.*, 30(4):1048–1057, Jul./Aug. 1994.
- [6] T. Laczynski, T. Werner, and A. Mertens. Energy-based modulation error control for high-power drives with output LC-filters and synchronous optimal pulse width modulation. In *Proc. IEEE Power Electron. and Motion Control Conf.*, pages 649–656, Sep. 2008.
- [7] B. Beyer. *Schnelle Stromregelung für Hochleistungsantriebe mit Vorgabe der Stromtrajektorie durch off-line optimierte Pulsmuster*. PhD thesis, Wuppertal University, 1998.
- [8] J. Holtz and N. Oikonomou. Synchronous optimal pulsewidth modulation and stator flux trajectory control for medium-voltage drives. *IEEE Trans. Ind. Appl.*, 43(2):600–608, Mar./Apr. 2007.
- [9] N. Oikonomou and J. Holtz. Stator flux trajectory tracking control for high-performance drives. In *Proc. IEEE Ind. Appl. Soc. Annu. Mtg.*, volume 3, pages 1268–1275, Tampa, FL, USA, Oct. 2006.
- [10] N. Oikonomou and J. Holtz. Estimation of the fundamental current in low-switching-frequency high dynamic medium-voltage drives. *IEEE Trans. Ind. Appl.*, 44(5):1597–1605, Sep./Oct. 2008.
- [11] C. E. Garcia, D. M. Prett, and M. Morari. Model predictive control: Theory and practice—A survey. *Automatica*, 25(3):335–348, Mar. 1989.
- [12] D. Q. Mayne, J. B. Rawlings, C. V. Rao, and P. O. M. Scokaert. Constrained model predictive control: Stability and optimality. *Automatica*, 36(6):789–814, Jun. 2000.
- [13] J. B. Rawlings and D. Q. Mayne. *Model predictive control: Theory and design*. Nob Hill Publ., Madison, WI, USA, 2009.
- [14] A.K. Rathore, J. Holtz, and T. Boller. Synchronous optimal pulsewidth modulation for low-switching-frequency control of medium-voltage multilevel inverters. *IEEE Trans. Ind. Electron.*, 57(7):2374–2381, Jul. 2010.
- [15] D. G. Holmes and T. A. Lipo. *Pulse width modulation for power converters: principles and practice*. IEEE Press, 2003.
- [16] J. Nocedal and S. J. Wright. *Numerical Optimization*. Springer, New York, 1999.
- [17] T. Geyer, G. Papafotiou, and M. Morari. Model predictive direct torque control—Part I: Concept, algorithm and analysis. *IEEE Trans. Ind. Electron.*, 56(6):1894–1905, Jun. 2009.
- [18] T. Geyer. Generalized model predictive direct torque control: Long prediction horizons and minimization of switching losses. In *Proc. IEEE Conf. Decis. Control*, pages 6799–6804, Shanghai, China, Dec. 2009.
- [19] T. Geyer. Computationally efficient model predictive direct torque control. *IEEE Trans. Power Electron.*, 26(10):2804–2816, Oct. 2011.
- [20] B. P. McGrath, D. G. Holmes, and T. Lipo. Optimized space vector switching sequences for multilevel inverters. *IEEE Trans. Power Electron.*, 18(6):1293–1301, Nov. 2003.